applied sciences

MDPI

Article

Study on the Population Balance Dynamics Simulation of Grinding under Impact Crushing

Shaojian Ma [1,2,3], Xiaojing Yang [2], Hengjun Li [2], Zongyu Li [1], Pengyan Zhu [2] and Jinlin Yang [1,*]

[1] State Key Laboratory of Featured Metal Materials and Life-Cycle Safety for Composite Structures, MOE Key Laboratory of New Processing Technology for Nonferrous Metals, Guangxi Higher School Key Laboratory of Minerals Engineering and Materials, College of Resources, Environment and Materials, Guangxi University, Nanning 530004, China; 1615391004@alu.gxu.edu.cn (S.M.); 2215394012@st.gxu.edu.cn (Z.L.)
[2] College of Chemistry and Chemical Engineering, Guangxi University, Nanning 530004, China; kjcyxj@gxu.edu.cn (X.Y.); 1615302001@st.gxu.edu.cn (H.L.); zpyandjyy@163.com (P.Z.)
[3] Hechi University, Guangxi, Hechi 546300, China
* Correspondence: jlyang523@126.com; Tel.: +86-131-5266-0958

Abstract: During the grinding process, the crushing of minerals mainly depends on the impact action of the grinding medium. Based on the JK drop weight test data of quartz and pyrrhotite and the research results of their impact crushing characteristic parameters, this paper calculates the specific crushing energy (E_{cs}) of mineral samples subjected to impact in a ball mill using the grinding medium motion theory and then calculates the cumulative particle size distribution under screening under any mesh size using the JK drop weight test method. On this basis, the breakage distribution function of mineral samples is calculated, and a selection function is obtained based on grinding experiments. Finally, using Matlab programming and function-fitting mathematical methods, as well as a particle size population balance dynamics simulation of grinding, the particle size distribution characteristics of the grinding products of the two mineral samples in the mill that are only subjected to impact action are calculated. The results show that the selection function of quartz and pyrrhotite decreases overall with the prolongation of the grinding time, and the selection function of the coarse particle size changes more significantly than that of the fine particle size. At the same time, the selection function decreases with the decrease in feed particle size, and the smaller the feed particle size, the lower the probability of impact crushing. The E_{cs} values of quartz and pyrrhotite at each particle level in the mill are different, and the degree of mineral crushing is closely related to the impact energy, feed particle size, and mineral properties.

Keywords: grinding; impact action; population balance dynamics; breakage distribution function; select function

Citation: Ma, S.; Yang, X.; Li, H.; Li, Z.; Zhu, P.; Yang, J. Study on the Population Balance Dynamics Simulation of Grinding under Impact Crushing. *Appl. Sci.* **2024**, *14*, 5455. https://doi.org/10.3390/app14135455

Academic Editor: Arkadiusz Gola

Received: 12 May 2024
Revised: 15 June 2024
Accepted: 21 June 2024
Published: 24 June 2024

1. Introduction

Grinding operations, which diminish the particle size of minerals, are applied extensively across various sectors to process solid mineral resources, including mining, chemical engineering, metallurgy, and the production of construction materials [1–3]. Grinding operations are crucial in the mineral processing industry, in which the investment in infrastructure constitutes approximately 60% of the total construction expenses for a mineral processing facility, and operational costs contribute to around 40% to 50% of the overall expenses of a plant [4–6]. In terms of mineral processing, grinding is the most energy-consuming operation [7,8]. As mineral resources are increasingly extracted and utilized, the ore grade diminishes, leading to a gradual decline in the overall quality of the resources available. The mineral deposits that were once rich in grade, accessible, amenable to grinding, and straightforward to beneficiate are increasingly exhausted, giving way to lower-grade and intricate ore bodies [9,10]. These ores, characterized by their heterogeneity and the diversity of their mineral constituents, present substantial variations in their

physical and chemical attributes [11,12]. Such complexity poses significant challenges to the efficiency of the grinding separation processes and impacts the economic and technical performance of the concentration plant [13,14]. Operating conditions such as grinding concentration, grinding time, filling rate, and rotational speed can also significantly affect the grinding process [15–17]. Therefore, optimizing grinding operations, delving into grinding theory, enhancing the efficiency of grinding operations, and cutting down on grinding costs are pivotal in slashing production expenses and improving the efficiency of resource recycling and usage [18–21].

Grinding behavior is a process in which numerous solid particles continuously rupture under the continuous or periodic external force of the grinding medium. The breakage results of solid particles are closely related to various factors such as the strength of solid particles to resist damage, manner and magnitude of external forces, direction of the application of forces, time of application, particle flow velocity, and particle size distribution of the particle groups. Therefore, grinding behavior and the grinding process are the most fundamental, critical, and intricate scientific challenges in formulating a comprehensive grinding theory. With the progress of modern scientific and technological research methods and means, the means and capabilities of grinding research have been strengthened, further enriching the analytical theory of grinding. The concept of population balance dynamics simulations of grinding is proposed based on statistical changes in terms of quantity particles in the grinding process. Many scholars have carried out a lot of work to improve models for different grinding environments [22–30]. Nikolov devised a performance model for impact crushers, and their simulation outcomes align closely with experimental data, indicating that an increase in rotor speed leads to a finer product size distribution, assuming the feed rate and particle size remain constant [31]. Shi conducted an overview of the various applications of the JK size-dependent breakage model [32]. Deniz examined the influence of varying mill speeds on the grinding behavior of diverse particulate pumice samples under batch-grinding scenarios, utilizing a kinetic model as the framework for their analysis [33]. Umucu investigated the breakage behavior of three distinct coal types in a laboratory impact crusher, and a new model was developed and tested by a t-family value evaluation and the Bond grindability approach and model [34]. However, whether the population balance dynamics simulation of grinding can really be used well or not, the key is building a good breakage rate function to describe the proportion of particle crushing mass and a breakage distribution function to describe the particle size distribution of crushing products and finding an effective solution. In addition, previous studies have shown that different material properties also exhibit different breakage behaviors, and the corresponding matrix and kinetic grinding models may also be different.

On the basis of the above introduction, this paper selects quartz and pyrrhotite, two ores with different properties, for research. This paper's aim is to investigate the contribution of a media ball's impact to ore breakage. In the throwing state, the media ball only has an impact on the ore. The current research work separates the impact and grinding effects and conducts a population balance dynamics simulation separately. It aims to simplify the complex grinding process through the means of the population balance dynamics simulation of grinding under impact crushing and provide a theoretical and data basis for subsequent grinding research. The ultimate goal is to obtain the optimal grinding conditions, while saving energy and maximizing the production efficiency of grinding.

2. Materials and Methods

2.1. Materials

To investigate the impact crushing properties of single minerals, natural minerals such as quartz and pyrrhotite with higher levels of purity were acquired for use as experimental specimens. After crushing, sieving, and mixing the test sample, it is ready for use in subsequent tests. In this paper, a sieve ratio of $\sqrt{2}$ is used to divide the product particle size into 13 particle sizes, including −3.35 + 2.36 mm, −2.36 + 1.7 mm, −1.7 + 1.18 mm, −1.18 + 0.85 mm, −0.85 + 0.6 mm, −0.6 + 0.425 mm, −0.425 + 0.3 mm, −0.3 + 0.212 mm,

−0.212 + 0.15 mm, −0.15 + 0.106 mm, −0.106 + 0.075 mm, −0.075 + 0.038 mm, and −0.038 mm. During calculation, the geometric average of the upper and lower limits of each particle size (i.e., nominal particle size) is used to characterize each product particle size. To facilitate subsequent calculations, it is assumed that the boundary particle size of the smallest particle size is 0.01 mm. Semiquantitative testing was conducted on the two minerals, and the elemental analysis results are shown in Tables 1 and 2.

Table 1. Chemical components of quartz.

Component	**SiO_2**	**Fe_2O_3**	**MgO**	**Al_2O_3**	**S**	**CaO**
Content/%	99.15	0.49	0.12	0.081	0.065	0.062
Component	**Mn**	**Cr**	**Ni**	**Cu**	**Zn**	**Others**
Content/%	0.0059	0.0047	0.0038	0.0035	0.0022	0.0119

Table 2. Chemical components of pyrrhotite.

Component	**SiO_2**	**CaO**	**Fe**	**Zn**	**S**	**Pb**
Content/%	29.41	0.18	37.76	0.94	25.94	0.18
Component	**Al_2O_3**	**As**	**K_2O**	**Pb**	**Others**	
Content/%	1.85	3.34	0.20	0.18	0.02	

From Table 1, it can be seen that 99.15% of the chemical composition of quartz is silicon dioxide, indicating that the purity of quartz is very high and the content of impurities is low. It can be seen from Table 2 that the content of iron element in pyrrhotite reaches 37.76%, and the content of sulfur element reaches 25.94%, which is typical of a sulfide mineral.

2.2. Methods

2.2.1. JK Drop Weight Test [35]

The JK drop weight testing equipment used in this article is a falling weight testing machine developed by the JK Mineral Research Center (JKMRC) of the University of Queensland, Brisbane, QLD, Australia. Quartz and pyrrhotite were screened into five particle sizes: −63 + 53 mm, −45 + 37.5 mm, −31.5 + 26.5 mm, −22.4 + 19 mm, and −16 + 13.2 mm, with representative particles chosen from each category of particle size for testing. The number of particles corresponding to the five particle sizes is 30, 45, 90, 90, and 90. Then minerals were divided into three equal parts for each particle size, totaling 15 parts.

According to the screening analysis of impact crushing products and the calculation method provided by JKMRC, the respective impact crushing parameters A and b for the two mineral types can be determined individually. Based on particle size analysis of quartz and pyrrhotite impact crushing products, particle size characteristic curves can be plotted. Using the Origin function to fit the regression analysis, the DoseResp particle size distribution model for mineral impact crushing products can be obtained, as shown in Equation (1) [36]. Therefore, the cumulative particle size distribution under sieve for any desired particle size can be calculated.

$$y = A_1 + \frac{A_2 - A_1}{1+10^{(logx_0 - x)\cdot p}} \quad (1)$$

where x is the sieving particle size (mm), and y is the corresponding cumulative weight undersize percentage (%), A_1 and A_2 are the upper and lower asymptotes of the particle size characteristic curve (%), $logx_0$ is the particle size at $(A_1 + A_2)/2$(mm), and p is the absolute value of the maximum slope on the particle size curve (%/mm).

Utilizing the established DoseResp particle size distribution model, the cumulative particle size distribution under sieve for any specific mesh size from the products of

15 crushing tests on individual minerals can be calculated. Generally, a particle size within the crushed product that is smaller than one tenth of the original feed particle size is designated as the characteristic particle size. The cumulative particle size distribution under sieve corresponding to this characteristic particle size reflects the degree of crushing of the mineral and is labeled t_{10}. Similarly, in the subsequent description, t_{xx} is used to represent the cumulative mass percentage of particles in the crushing product whose particle size is less than 1/xx of the feed particle size. Utilizing the 15 datasets of t_{10} values and E_{cs}, a scatter diagram illustrating the correlation between t_{10} and E_{cs} can be constructed. Subsequent fitting analysis of this t_{10}-E_{cs} relationship allows for the determination of the mineral's impact crushing characteristic parameters A and b, as represented in Equation (2).

$$t_{10} = A\left(1 - e^{-b \cdot E_{cs}}\right) \tag{2}$$

The t_{10}-E_{cs} correlation was initially proposed by Leung [37] and subsequently validated by Napier Munn et al. [38] based on the existence of a certain relationship between particle size distribution and specific crushing energy after mineral crushing. This correlation holds considerable importance for engineering applications. Since the $t_{10}E_{cs}$ relationship remains consistent across different grinding equipment [39], and the parameters A and b are solely governed by the mineral's intrinsic properties, this relationship is applicable for the selection and refinement of grinding equipment. For the convenience of our research, Equation (2) is abbreviated to the particle energy relationship equation of the material in the following description.

2.2.2. Batch-Grinding Test

The batch-grinding test used a cylindrical ball mill with a size of 200 mm × 400 mm. In the test, in order to keep the grinding medium performing a throwing impact action, the rotational speed is adjusted to 92 1/min, which is 90.7% of the critical rotational speed. The medium filling ratio was 35%, the grinding concentration was 75%, and the steel ball diameter was 25 mm. The grinding results of three different feed particle sizes (−3.35 + 2.36 mm, −2.36 + 1.7 mm, and −1.7 + 1.18 mm) at different grinding times (including 0.5 min, 1 min, 2 min, 4 min, and 8 min) were investigated.

2.2.3. Calculation of the E_{cs} of Particles in Grinding with Throwing State

E_{cs} refers to the impact energy per unit mass of the ores. Many scholars [40,41] have conducted systematic research on the impact energy of the drop type movement of media in a mill and obtained the formula for calculating the E_{cs} of the drop type movement of media as Equation (3).

$$E_{cs} = \frac{m}{2M}\left(\frac{n^2\pi^2R^2}{30^2} + \frac{3.0127n\pi R}{30}\sqrt{gR}\right) \tag{3}$$

In Equation (3), m is the mass of the steel ball, M is the mass of the mineral material, n is the rotational speed of the mill, and R is the radius of the mill.

2.2.4. Calculation of Breakage Distribution Function

According to the definition of breakage distribution function by Narayanan, Pauw, and Bourgeois et al. [42–44], the relationship between the elements B_{ij} and b_{ij} is shown in Equation (4) [45]. According to the definition of B_{ij}, each element B_{ij} corresponds to a t_{xx} value, and a series of t_{xx} values constitute the cumulative distribution matrix of ore impact crushing.

When ore is broken only by impact, the breakage distribution matrix b_{ij} of the ore under impact energy can be calculated according to Equations (4) and (5), where the element b_{ij} is the complete particle size distribution value of the ore.

$$B_{ij} = \sum_{k=1}^{i} b_{kj} \tag{4}$$

$$b_{kj} = B_{ij} - B_{i+1,j} (1 \le j \le i \le N) \quad (5)$$

In Equation (4), B_{ij} refers to the cumulative particle size distribution of particles generated by j particle crushing that are smaller than the upper limit size of i particle crushing, and b_{ij} refers to the yield of j particle crushing that generates i particles.

Equation (5) shows that the mass fraction of i particles generated from j particle crushing is equal to the mass fraction of j particles, which can be broken further down to the mass fraction of i particles minus the fraction of mass broken down to fewer than $i + 1$ particles.

2.2.5. Calculation of the Selection Function

The calculation of the selection function S_i can be completed using the zero-order output rate method proposed by Herbst [46], as shown in Equation (6) below:

$$S_i = S_1 \frac{\sqrt{x_i x_{i+1}}}{\sqrt{x_1 x_2}} \quad (6)$$

In the formula, S_1 represents the selection function of the first particle level, and S_i represents the selection function of the ith particle level.

3. Results and Discussion

3.1. The Population Balance Dynamics Simulation of Grinding under Impact Crushing of Quartz

3.1.1. Calculate the Cumulative Particle Size Distribution under Sieve t_{xx} for Any Sieve Size Based on the Drop Weight Test Results

Based on the data obtained from the drop weight test in Section 2.2.1, the calculated xx value is used as a subscript for the cumulative particle size distribution under the sieve, and the results shown in Table 3 are obtained.

According to Section 2.2.1, based on the quartz drop weight test data, we used the interpolation method to obtain points of the cumulative particle size distribution curve under the sieve and calculated the t_{xx} values listed in Table 3. On this basis, we drew a scatter relationship diagram between the t_{xx} value and the corresponding groups of t_{10} values, as shown in Figure 1. Using the Origin polynomial-fitting method, the functional relationship between t_{10}-t_{xx} of the quartz under impact is obtained, as shown in Table 4. According to this, given any value of t_{10}, the corresponding series of t_{xx} values can be calculated, that is, the cumulative particle size distribution under the sieve for different particle sizes.

Table 4 reveals that the R^2 values of all t_{xx} are close to 1, higher than the R^2 value of Deniz [47], and similar to the R^2 values of Genç [48,49], Deniz [50], and Mulenga [51], indicating that the data in this study have a high level of reliability. The above t_{10}-t_{xx} function relationship is obtained under the impact of the drop weight test and is only related to the properties of mineral samples. When the quartz is broken in the mill, E_{cs} can be calculated based on Section 2.2.3. Based on Equation (2), the corresponding t_{10} value for each particle size in the mill can be calculated. Combining the t_{10}-t_{xx} function relationship in Table 4, a series of t_{xx} values under any t_{10} can be obtained. Therefore, a complete particle size distribution can be obtained.

According to Sections 2.2.1 and 2.2.3, the calculated results of the E_{cs} and t_{10} values for each particle size are shown in Table 5.

From Table 5, it can be seen that the E_{cs} of the 25 mm steel ball media for 2.8118 mm quartz particles in a cylindrical ball mill reaches 1.39 kWh/t, which can lead to its t_{10} reaching 46.35%. When the quartz particle is 1.0015 mm, its E_{cs} is 30.97 kWh/t, which can lead to its t_{10} reaching the limit value of 67.33%. As the particle size continues to decrease, the E_{cs} of the particles increases, but the degree of fragmentation does not increase. This is because finer particle sizes demand greater energy inputs for comminution and there is a smaller probability of contact with the steel ball, so its t_{10} no longer increases with the increase in the E_{cs} received.

Table 3. The ratio of the product particle size produced by the crushing of each sieve particle size.

Product Particle Size/mm	Nominal Particle Size/mm	Nominal Particle Size/mm												
		2.8118	**2.003**	**1.4163**	**1.0015**	**0.7141**	**0.5050**	**0.3571**	**0.2522**	**0.1783**	**0.1261**	**0.0892**	**0.0630**	**0.0449**	**0.0195**
−3.35 + 2.36	2.8118	$t_{1.0}$													
−2.36 + 1.7	2.003	$t_{1.4}$	$t_{1.0}$												
−1.7 + 1.18	1.4163	$t_{2.0}$	$t_{1.4}$	$t_{1.0}$											
−1.18 + 0.85	1.0015	$t_{2.8}$	$t_{2.0}$	$t_{1.4}$	$t_{1.0}$										
−0.85 + 0.60	0.7141	$t_{3.9}$	$t_{2.8}$	$t_{2.0}$	$t_{1.4}$	$t_{1.0}$									
−0.6 + 0.425	0.5050	$t_{5.6}$	$t_{4.0}$	$t_{2.8}$	$t_{2.0}$	$t_{1.4}$	$t_{1.0}$								
−0.425 + 0.3	0.3571	$t_{7.9}$	$t_{5.6}$	$t_{4.0}$	$t_{2.8}$	$t_{2.0}$	$t_{1.4}$	$t_{1.0}$							
−0.3 + 0.212	0.2522	$t_{11.1}$	$t_{7.9}$	$t_{5.6}$	$t_{4.0}$	$t_{2.8}$	$t_{2.0}$	$t_{1.4}$	$t_{1.0}$						
−0.212 + 0.15	0.1783	$t_{15.8}$	$t_{11.2}$	$t_{7.9}$	$t_{5.6}$	$t_{4.0}$	$t_{2.8}$	$t_{2.0}$	$t_{1.4}$	$t_{1.0}$					
−0.15 + 0.106	0.1261	$t_{22.3}$	$t_{15.9}$	$t_{11.2}$	$t_{7.9}$	$t_{5.7}$	$t_{4.0}$	$t_{2.8}$	$t_{2.0}$	$t_{1.4}$	$t_{1.0}$				
−0.106 + 0.075	0.0892	$t_{31.5}$	$t_{22.5}$	$t_{15.9}$	$t_{11.2}$	$t_{8.0}$	$t_{5.7}$	$t_{4.0}$	$t_{2.8}$	$t_{2.0}$	$t_{1.4}$	$t_{1.0}$			
−0.075 + 0.053	0.0630	$t_{44.6}$	$t_{31.8}$	$t_{22.5}$	$t_{15.9}$	$t_{11.3}$	$t_{8.0}$	$t_{5.7}$	$t_{4.0}$	$t_{2.8}$	$t_{2.0}$	$t_{1.4}$	$t_{1.0}$		
−0.053 + 0.038	0.0449	$t_{62.6}$	$t_{44.6}$	$t_{31.5}$	$t_{22.3}$	$t_{15.9}$	$t_{11.2}$	$t_{8.0}$	$t_{5.6}$	$t_{4.0}$	$t_{2.8}$	$t_{2.0}$	$t_{1.4}$	$t_{1.0}$	
−0.038 + 0.013	0.0195	$t_{144.2}$	$t_{102.8}$	$t_{72.7}$	$t_{51.4}$	$t_{36.6}$	$t_{25.9}$	$t_{18.3}$	$t_{12.9}$	$t_{9.15}$	$t_{6.5}$	$t_{4.6}$	$t_{2.0}$	$t_{1.4}$	$t_{1.0}$

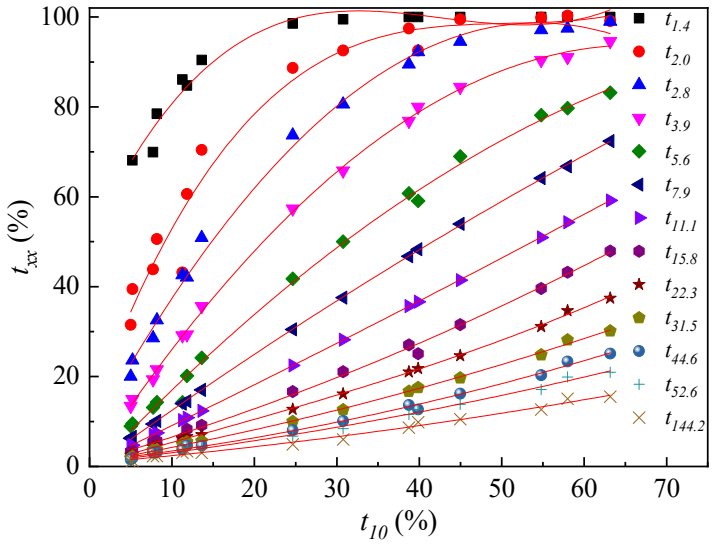

Figure 1. The relation curves of t_{10}-t_{xx} for quartz.

Table 4. Functional relation of t_{10}-t_{xx} for quartz.

t_{xx}	Fitting Equation	R^2
$t_{1.4}$	$t_{1.4} = 50.3655 + 3.9373t_{10} - 0.0976{t_{10}}^2 + 7.6231 \times 10^{-4}{t_{10}}^3$	0.9582
$t_{2.0}$	$t_{2.0} = 11.5492 + 5.0587t_{10} - 0.0988{t_{10}}^2 + 6.4790 \times 10^{-4}{t_{10}}^3$	0.9584
$t_{2.8}$	$t_{2.8} = 6.7042 + 3.3822t_{10} - 0.0311{t_{10}}^2$	0.9953
$t_{3.9}$	$t_{3.9} = -0.0723 + 2.8244t_{10} - 0.0213{t_{10}}^2$	0.9991
$t_{5.6}$	$t_{5.6} = -1.7103 + 1.97t_{10} - 0.0097{t_{10}}^2$	0.9958
$t_{7.9}$	$t_{7.9} = -0.53 + 1.33t_{10} - 0.0028{t_{10}}^2$	0.9999
$t_{11.1}$	$t_{11.1} = 0.1882 + 0.8837t_{10} + 8.0415 \times 10^{-4}{t_{10}}^2$	1
$t_{15.8}$	$t_{15.8} = 0.9599 + 0.5256t_{10} + 0.0033{t_{10}}^2$	0.9969
$t_{22.3}$	$t_{22.3} = 0.2401 + 0.514t_{10} - 6.9004 \times 10^{-4}{t_{10}}^2 + 3.1204 \times 10^{-5}{t_{10}}^3$	0.9991
$t_{31.5}$	$t_{31.5} = 0.8033 + 0.3217t_{10} + 0.0023{t_{10}}^2$	0.9980
$t_{44.6}$	$t_{44.6} = 1.0755 + 0.2106t_{10} + 0.0027{t_{10}}^2$	0.9952
$t_{62.6}$	$t_{62.6} = 0.7647 + 0.2124t_{10} + 0.0018{t_{10}}^2$	0.9945
$t_{144.2}$	$t_{144.2} = 0.7007 + 0.1579t_{10} + 0.0013{t_{10}}^2$	0.9877

Table 5. The calculated results of the E_{cs} and t_{10} values for each particle size of quartz.

Particle Size/mm	Nominal Particle Size/mm	M/kg	E_{cs}/kWh/t	t_{10}/%
−3.35 + 2.36	2.8118	3.0830×10^{-5}	1.3994	46.3585
−2.36 + 1.7	2.003	1.1145×10^{-5}	3.8713	64.6617
−1.7 + 1.18	1.4163	3.9399×10^{-6}	10.9505	67.3277
−1.18 + 0.85	1.0015	1.3931×10^{-6}	30.9705	67.3350
−0.85 + 0.60	0.7141	5.0501×10^{-7}	85.4327	67.3350
−0.6 + 0.425	0.5050	1.7861×10^{-7}	241.5610	67.3350
−0.425 + 0.3	0.3571	6.3153×10^{-8}	683.1742	67.3350
−0.3 + 0.212	0.2522	2.2246×10^{-8}	1.9394×10^{3}	67.3350
−0.212 + 0.15	0.1783	7.8610×10^{-9}	5.4884×10^{3}	67.3350
−0.15 + 0.106	0.1261	2.7808×10^{-9}	1.5515×10^{4}	67.3350
−0.106 + 0.075	0.0892	9.8428×10^{-10}	4.3834×10^{4}	67.3350
−0.075 + 0.053	0.0630	3.4677×10^{-10}	1.2442×10^{5}	67.3350
−0.053 + 0.038	0.0449	1.2554×10^{-10}	3.4369×10^{5}	67.3350
−0.038 + 0.010	0.0195	1.0273×10^{-11}	4.1998×10^{6}	67.3350

3.1.2. Calculation of Breakage Distribution Function

In Table 5, the E_{cs} and corresponding t_{10} values of the quartz with different particle sizes in the mill are given. Combining the t_{10}-t_{xx} function relationship, a series of t_{xx} values for different particle sizes can be obtained, that is, the element B_{ij} of the cumulative breakage distribution matrix $\boldsymbol{B_{ij}}$ of the quartz. According to Equation (5), the breakage

distribution function b_{ij} of the quartz can be obtained, which is the complete particle size distribution of the quartz under the impact of the steel ball media, as shown in Table 6.

Table 6. The b_{ij} matrix of quartz under impact crushing.

Particle Size/mm	Nominal Particle Size/mm												
	2.8118	**2.003**	**1.4163**	**1.0015**	**0.7141**	**0.5050**	**0.3571**	**0.2522**	**0.1783**	**0.1261**	**0.0892**	**0.0630**	**0.0449**
−3.35 + 2.36	0.0001												
−2.36 + 1.7	0.0012	0.0000											
−1.7 + 1.18	0.0096	0.0012	0.0001										
−1.18 + 0.85	0.0858	0.0096	0.0012	0.0000									
−0.85 + 0.60	0.0010	0.0858	0.0096	0.0012	0.0002								
−0.6 + 0.425	0.0657	0.0010	0.0858	0.0096	0.0012	0.0001							
−0.425 + 0.3	0.1063	0.0657	0.0010	0.0858	0.0096	0.0012	0.0000						
−0.3 + 0.212	0.1299	0.1063	0.0657	0.0010	0.0858	0.0096	0.0012	0.0000					
−0.212 + 0.15	0.1202	0.1299	0.1063	0.0657	0.0010	0.0858	0.0096	0.0012	0.0002				
−0.15 + 0.106	0.1007	0.1202	0.1299	0.1063	0.0657	0.0010	0.0858	0.0096	0.0012	0.0000			
−0.106 + 0.075	0.0835	0.1007	0.1202	0.1299	0.1063	0.0657	0.0010	0.0858	0.0096	0.0012	0.0000		
−0.075 + 0.053	0.0540	0.0835	0.1007	0.1202	0.1299	0.1063	0.0657	0.0010	0.0858	0.0096	0.0012	0.0001	
−0.053 + 0.038	0.0427	0.0540	0.0835	0.1007	0.1202	0.1299	0.1063	0.0657	0.0010	0.0858	0.0096	0.0012	0.0000
−0.038 + 0.013	0.0600	0.0427	0.0540	0.0835	0.1007	0.1202	0.1299	0.1063	0.0657	0.0010	0.0858	0.0096	0.0012

Table 6 lists the breakage distribution function $\boldsymbol{b_{ij}}$ of the quartz only under impact, and each element b_{ij} in the matrix represents the yield of particle size i generated by particle size j fragmentation. In a mill, the i particle size originates from the crushing of any particle size coarser than it, while the j particle size will be crushed to produce a finer particle size.

3.1.3. Calculation of the Selection Function

Based on the batch-grinding test data, according to Section 2.2.5, the selection function S_i for each particle size of quartz with a feed particle size of 3.35 + 2.36 mm, −2.36 + 1.7 mm, and −1.7 + 1.18 mm is calculated. The relationship curve between the selection function and time is shown in Figure 2.

According to Figure 2, the selection function of each particle size of quartz generally shows a downward trend with time. The selection function of the coarse particle size is higher than that of the fine particle size. This is because the larger the particle size, the greater the chance of contact with the steel ball medium and the higher the probability of being broken. In addition, the selection functions of the three feed particle sizes were significantly higher than those of the other product particle sizes. This is because after the feed particle size enters the mill, it is in full contact with the steel ball medium and has the highest probability of being crushed by impact, so the selection function is the highest. Except for the feed particle size, other product particle sizes need to increase with the grinding time before they can be further broken by steel balls, so their selection function is significantly lower than the feed particle size. It can also be seen from Figure 2 that the selection function exhibits a decline with the reduction in feed particle size. This is because the smaller the particle size, the greater the energy required to be broken. And the smaller the particle size, the less chance of contact with the steel ball, so the lower the probability of being broken.

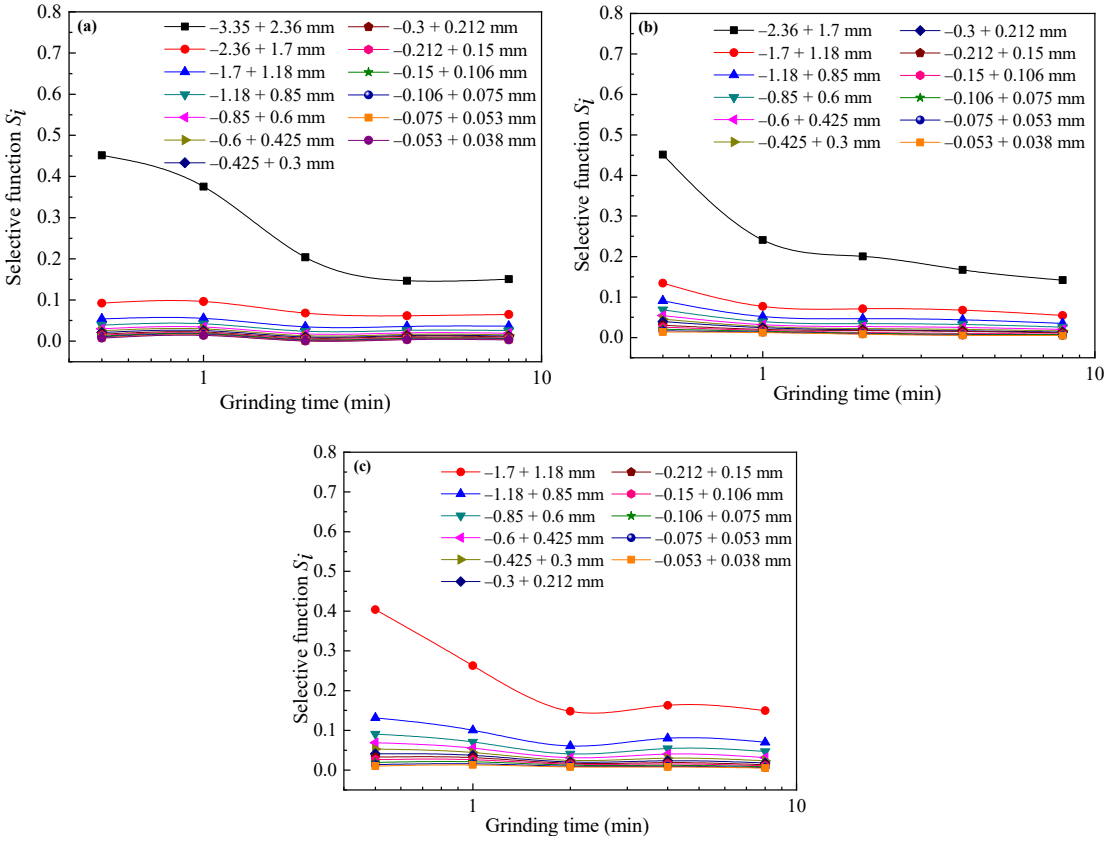

Figure 2. The relationship curve between the S_i and time of quartz: (**a**) −3.35 + 2.36 mm, (**b**) −2.36 + 1.7 mm, (**c**) −1.7 + 1.18 mm.

3.1.4. Study on Simulation Results of the Population Balance Dynamics of Grinding for Quartz

Based on the obtained breakage distribution function b_{ij} and selection function S_i of the quartz, combined with the Reid solution of the grinding overall balance equation [26], the yield of each product particle size generated by crushing the quartz under impact is calculated using MATLAB2018a programming. The variation in product yield with time for the quartz with the feed particle size of 3.35 + 2.36 mm is shown in Figure 3.

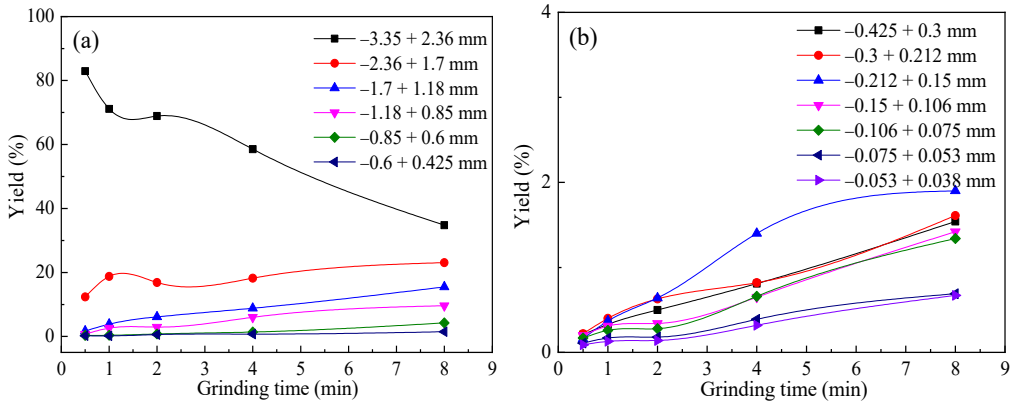

Figure 3. The variation in product yield with time for quartz with the feed particle size of 3.35 + 2.36 mm: (**a**) +0.425 mm particle size, (**b**) −0.425 mm particle size.

It can be seen from Figure 3 that the quartz with the feed particle size of −3.35 + 2.36 mm is crushed to products of various particle sizes after impact grinding. The yield of particle sizes of −2.36 + 1.7 mm, −1.7 + 1.18 mm, and −1.18 + 0.85 mm was higher, with the highest

yield of 23.09%, 15.5%, and 9.61%, respectively. The maximum yield observed for the remaining particle sizes is 4.25%. As depicted in Figure 3, when the ordinate range is large, the yield curve of the −0.85 + 0.6 mm particle size is very smooth. Upon magnification of the ordinate scale, as illustrated in Figure 3b, the yield of each particle size at the 8 min mark remains below 2%, and the yield curve is smoother. This indicates a notably low rate of fine particle production under impact.

Using the same method, we calculated the yield *Wi*(*t*) of the quartz with particle sizes of −2.36 + 1.7 mm and −1.7 + 1.18 mm broken into each particle size under impact action. The results are shown in Figures 4 and 5, respectively.

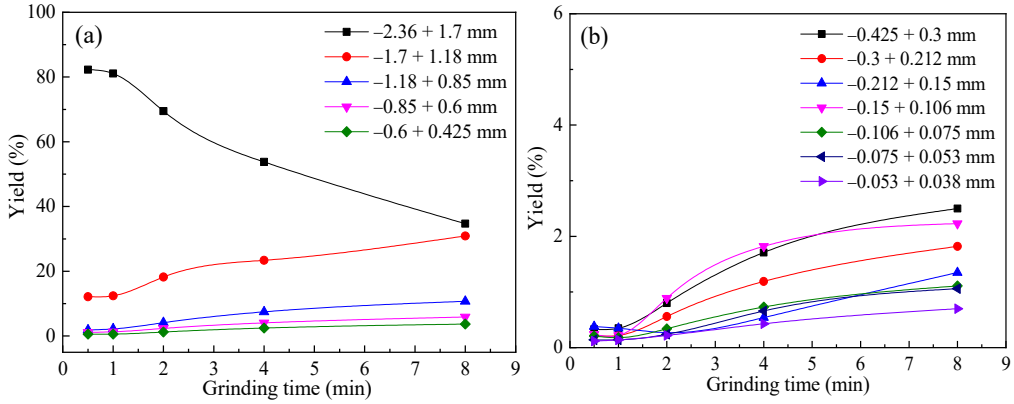

Figure 4. The variation in product yield with time for quartz with the feed particle size of −2.36 + 1.7 mm: (**a**) +0.425 mm particle size, (**b**) −0.425 mm particle size.

It can be seen from Figure 4 that with the feed particle size of −2.36 + 1.7 mm, the quartz is also crushed to products of various particle sizes after impact grinding. The highest yield of −1.7 + 1.18 mm and −1.18 + 0.85 mm particle sizes was 30.92% and 10.74%, respectively. The highest yield of other particle sizes is 5.86%. For the same product particle size, the yield of the −2.36 + 1.7 mm feed is higher than that of the −3.35 + 2.36 mm feed, and the generation rate is also faster. From the comparison between Figures 3b and 4b, it can be seen that the generation rate curve of the −0.425 mm particle sizes generated by impact grinding with a feed particle size of −2.36 + 1.7 mm has a significantly different trend compared to that of a feed particle size of −3.35 + 2.36 mm. This is because when the feed particle size decreases, the impact energy of the quartz becomes larger than the crushing energy, so the rate of crushing to generate various particle sizes is faster.

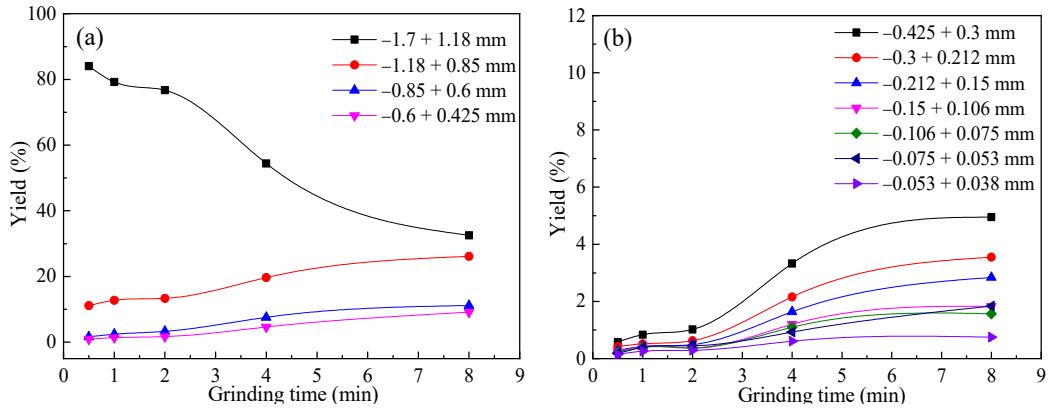

Figure 5. The variation in product yield with time for quartz with the feed particle size of −1.7 + 1.18 mm: (**a**) +0.425 mm particle size, (**b**) −0.425 mm particle size.

As can be seen from Figure 5, compared to Figures 3 and 4, the yield of each fine particle size broken from the quartz is the highest with the feed particle size of −1.7 + 1.18 mm.

The highest yields of the −1.18 + 0.85 mm and −0.85 + 0.6 mm particle sizes were 26.12% and 11.17%, respectively, while the highest yield of the other particle sizes were 9.14%. For the same product particle size, the yield of the −1.7 + 1.18 mm feed is higher than that of the −2.36 + 1.7 mm and −3.35 + 2.36 mm feeds. From a comparison between Figures 3b, 4b and 5b, it can be seen that the generation rate curve of the −1.7 + 1.18 mm feed particle sizes broken into −0.425 mm particle sizes has the most significantly different trend. This is because the feed particle size of −1.7 + 1.18 mm has the highest E_{cs} in the mill, reaching 10.95 kWh/t. The E_{cs} values of the −3.35 + 2.36 mm and −2.36 + 1.7 mm feeds are 1.40 kWh/t and 3.87 kWh/t, respectively. Therefore, the rate at which the quartz with the smallest particle size is broken into various fine particle sizes is the fastest.

3.2. The Population Balance Dynamics Simulation of Grinding under Impact Crushing of Pyrrhotite

3.2.1. Calculate the Cumulative Particle Size Distribution under Sieve t_{xx} for Any Sieve Size Based on the Drop Weight Test Results

Based on the data obtained from the drop weight test in Section 2.2.1, the calculated *xx* value is used as a subscript for the cumulative particle size distribution under the sieve, and the results shown in Table 3 of Section 3.1.1 are obtained.

According to Section 2.2.1, based on the pyrrhotite drop weight test data, we used the interpolation method to obtain the points for the cumulative particle size distribution curve under the sieve and calculated the t_{xx} values listed in Table 3 of Section 3.1.1. On this basis, we drew a scatter relationship diagram between the t_{xx} value and the corresponding groups of t_{10} values, as shown in Figure 6. Using the Origin polynomial-fitting method, the functional relationship between t_{10}-t_{xx} of the pyrrhotite under impact is obtained, as shown in Table 7.

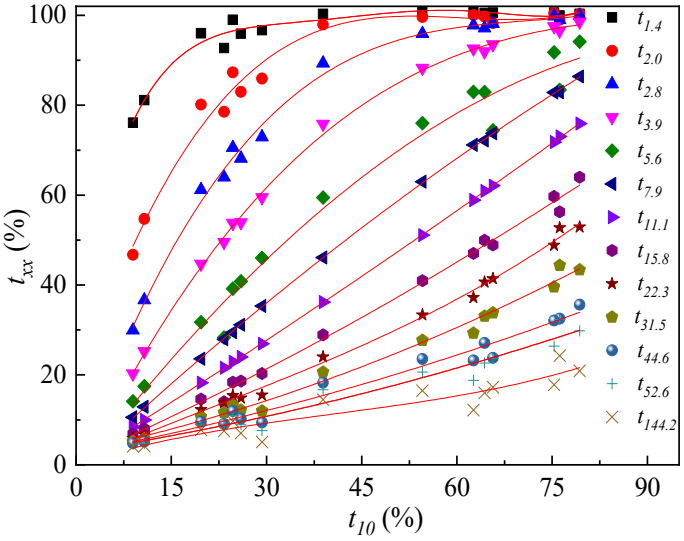

Figure 6. The relation curves of t_{10}-t_{xx} for pyrrhotite.

Like in Table 4, it can be seen from Table 7 that the R^2 values of all t_{xx} are close to 1, indicating that the test data have a high level of reliability. According to Sections 2.2.1 and 2.2.3, the calculated results of the E_{cs} and t_{10} values for each particle size are shown in Table 8.

From Table 8, it can be seen that the E_{cs} of the 25 mm steel ball medium for 2.8118 mm pyrrhotite particles is 0.81 kWh/t, and its t_{10} reaches 55.27%. When the particle size of pyrrhotite is 1.0015 mm, its E_{cs} is 17.84 kWh/t, which can lead to its t_{10} reaching the limit value of 76.59%. As the particle size continues to decrease, the E_{cs} of the particles increases, but the t_{10} does not increase. This correlation is attributable to the fact that finer particle sizes demand greater energy inputs for crushing and there is a reduced chance of contact with the steel ball, reducing the probability of being crushed. Therefore, its t_{10} no longer

increases with the increase in E_{cs}. Compared to the quartz particles, the pyrrhotite particles of the same size have a lower E_{cs}, but their t_{10} is larger and their crushing degree is higher. This means that minerals with lower hardness require less energy to be crushed by impact, which conforms to the mineral crushing principle.

Table 7. Functional relation of t_{10}-t_{xx} for pyrrhotite.

t_{xx}	Fitting Equation	R^2
$t_{1.4}$	$t_{1.4} = 33.3753 + 7.1239t_{10} - 0.3162{t_{10}}^2 + 0.007{t_{10}}^3 - 7.4178 \times 10^{-5}{t_{10}}^4 + 3.0379 \times 10^{-7}{t_{10}}^5$	0.9496
$t_{2.0}$	$t_{2.0} = 15.8714 + 4.2643t_{10} - 0.0713{t_{10}}^2 + 3.9037 \times 10^{-4}{t_{10}}^3$	0.9771
$t_{2.8}$	$t_{2.8} = -0.7524 + 3.9874t_{10} - 0.0546{t_{10}}^2 + 2.5608 \times 10^{-4}{t_{10}}^3$	0.9939
$t_{3.9}$	$t_{3.9} = -3.8249 + 2.9503t_{10} - 0.0283{t_{10}}^2 + 9.2259 \times 10^{-5}{t_{10}}^3$	0.9982
$t_{5.6}$	$t_{5.6} = -2.5216 + 1.8573t_{10} - 0.0082{t_{10}}^2 - 5.1016 \times 10^{-6}{t_{10}}^3$	0.9995
$t_{7.9}$	$t_{7.9} = -1.2380 + 1.3254t_{10} - 0.0028{t_{10}}^2$	0.9999
$t_{11.1}$	$t_{11.1} = 0.5161 + 0.8799t_{10} + 8.9764 \times 10^{-4}{t_{10}}^2$	1
$t_{15.8}$	$t_{15.8} = 0.997 + 0.6198t_{10} + 0.0019{t_{10}}^2$	0.9948
$t_{22.3}$	$t_{22.3} = 0.5455 + 0.6105t_{10} - 0.0027{t_{10}}^2 + 4.3588 \times 10^{-5}{t_{10}}^3$	0.9954
$t_{31.5}$	$t_{31.5} = 2.8650 + 0.3002t_{10} + 0.0027{t_{10}}^2$	0.9865
$t_{44.6}$	$t_{44.6} = 2.6921 + 0.2635t_{10} + 0.0017{t_{10}}^2$	0.9689
$t_{62.6}$	$t_{62.6} = 2.8678 + 0.2178t_{10} + 0.0016{t_{10}}^2$	0.9443
$t_{144.2}$	$t_{144.2} = 0.2106 + 0.4458t_{10} - 0.0064{t_{10}}^2 + 5.2529 \times 10^{-5}{t_{10}}^3$	0.8515

Table 8. The calculated results of the E_{cs} and t_{10} values for each particle size of pyrrhotite.

Particle Size/mm	Nominal Particle Size/mm	M/kg	E_{cs}/kWh/t	t_{10}/%
−3.35 + 2.36	2.8118	5.3517×10^{-5}	0.8062	55.2683
−2.36 + 1.7	2.003	1.9346×10^{-5}	2.2302	74.3688
−1.7 + 1.18	1.4163	6.8392×10^{-6}	6.3085	76.5951
−1.18 + 0.85	1.0015	2.4182×10^{-6}	17.8417	76.5986
−0.85 + 0.60	0.7141	8.7662×10^{-7}	49.2166	76.5986
−0.6 + 0.425	0.5050	3.1003×10^{-7}	139.1602	76.5986
−0.425 + 0.3	0.3571	1.0962×10^{-7}	393.5678	76.5986
−0.3 + 0.212	0.2522	3.8616×10^{-8}	1.1173×10^{3}	76.5986
−0.212 + 0.15	0.1783	1.3645×10^{-8}	3.1618×10^{3}	76.5986
−0.15 + 0.106	0.1261	4.8271×10^{-9}	8.9381×10^{3}	76.5986
−0.106 + 0.075	0.0892	1.7086×10^{-9}	2.5252×10^{4}	76.5986
−0.075 + 0.053	0.0630	6.0195×10^{-10}	7.1675×10^{4}	76.5986
−0.053 + 0.038	0.0449	2.1791×10^{-10}	1.9799×10^{5}	76.5986
−0.038 + 0.013	0.0195	1.7833×10^{-11}	2.4194×10^{6}	76.5986

3.2.2. Calculation of Breakage Distribution Function

The calculation process of the breakage distribution function of pyrrhotite is the same as that in Section 3.1.2, and the calculation results are shown in Table 9.

Table 9. The b_{ij} matrix of pyrrhotite under impact crushing.

Particle Size/mm	Nominal Particle Size/mm												
	2.8118	**2.003**	**1.4163**	**1.0015**	**0.7141**	**0.5050**	**0.3571**	**0.2522**	**0.1783**	**0.1261**	**0.0892**	**0.0630**	**0.0449**
−3.35 + 2.36	0.0001												
−2.36 + 1.7	0.0012	0.0000											
−1.7 + 1.18	0.0096	0.0012	0.0001										
−1.18 + 0.85	0.0858	0.0096	0.0012	0.0000									
−0.85 + 0.60	0.0010	0.0858	0.0096	0.0012	0.0002								
−0.6 + 0.425	0.0657	0.0010	0.0858	0.0096	0.0012	0.0001							
−0.425 + 0.3	0.1063	0.0657	0.0010	0.0858	0.0096	0.0012	0.0000						
−0.3 + 0.212	0.1299	0.1063	0.0657	0.0010	0.0858	0.0096	0.0012	0.0000					
−0.212 + 0.15	0.1202	0.1299	0.1063	0.0657	0.0010	0.0858	0.0096	0.0012	0.0002				
−0.15 + 0.106	0.1007	0.1202	0.1299	0.1063	0.0657	0.0010	0.0858	0.0096	0.0012	0.0000			
−0.106 + 0.075	0.0835	0.1007	0.1202	0.1299	0.1063	0.0657	0.0010	0.0858	0.0096	0.0012	0.0000		
−0.075 + 0.053	0.0540	0.0835	0.1007	0.1202	0.1299	0.1063	0.0657	0.0010	0.0858	0.0096	0.0012	0.0001	
−0.053 + 0.038	0.0427	0.0540	0.0835	0.1007	0.1202	0.1299	0.1063	0.0657	0.0010	0.0858	0.0096	0.0012	0.0000
−0.038 + 0.013	0.0600	0.0427	0.0540	0.0835	0.1007	0.1202	0.1299	0.1063	0.0657	0.0010	0.0858	0.0096	0.0012

3.2.3. Calculation of the Selection Function

The calculation process for the selection function is the same as that in Section 3.1.3. By batch grinding the test data, the relationship between the particle size selection function S_i and time for the pyrrhotite with different feed particle sizes is calculated as shown in Figure 7.

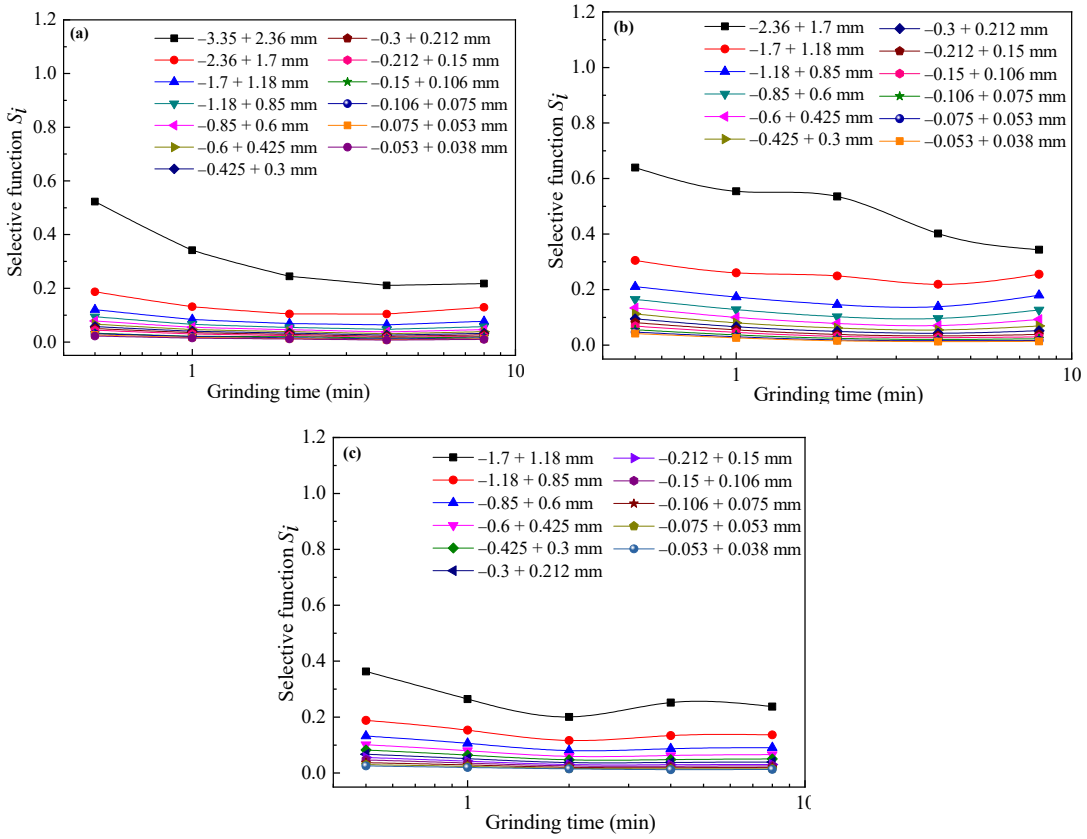

Figure 7. The relationship curve between the S_i and time of pyrrhotite: (**a**) −3.35 + 2.36 mm, (**b**) −2.36 + 1.7 mm, (**c**) −1.7 + 1.18 mm.

According to Figures 2 and 7, the selection functions for each particle size of pyrrhotite and quartz have similar characteristics. The selection function of each particle size shows

an overall downward trend over time, with the selection function of the coarse particle size being higher than that of the fine particle size. Moreover, the selection functions of the fine particle sizes are all small, and their changes over time are not particularly significant. And the selection functions of the fine particle sizes are even close to zero, indicating that the probability of them being selected for breakage is minimal. At the same time, Figure 7 further reveals that the selection function diminishes with a decrease in feed particle size.

3.2.4. Study on Simulation Results of the Population Balance Dynamics of Grinding for Pyrrhotite

As in Section 3.1.4, based on the obtained breakage distribution function b_{ij} and selection function S_i of pyrrhotite, combined with the Reid solution of the grinding overall balance equation [26], the yield of each product particle size generated by crushing the pyrrhotite under impact is calculated using MATLAB programming. The variation in the product yield with time for pyrrhotite with the feed particle size of 3.35 + 2.36 mm, −2.36 + 1.7 mm, and −1.7 + 1.18 mm is shown in Figures 8–10.

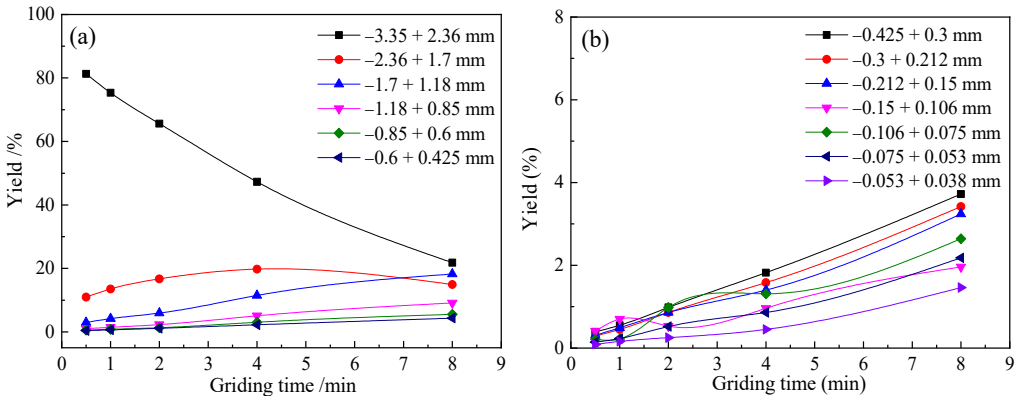

Figure 8. The variation in product yield with time for pyrrhotite with the feed particle size of 3.35 + 2.36 mm: (**a**) +0.425 mm particle size, (**b**) −0.425 mm particle size.

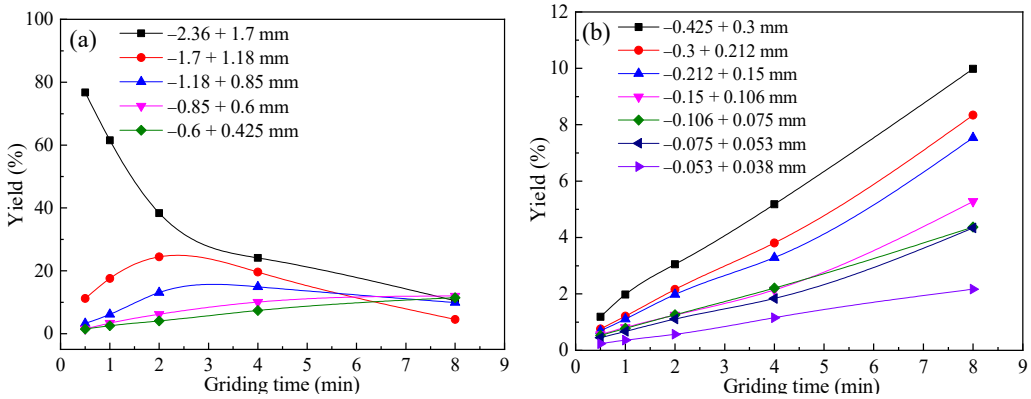

Figure 9. The variation in product yield with time for pyrrhotite with the feed particle size of −2.36 + 1.7 mm: (**a**) +0.425 mm particle size, (**b**) −0.425 mm particle size.

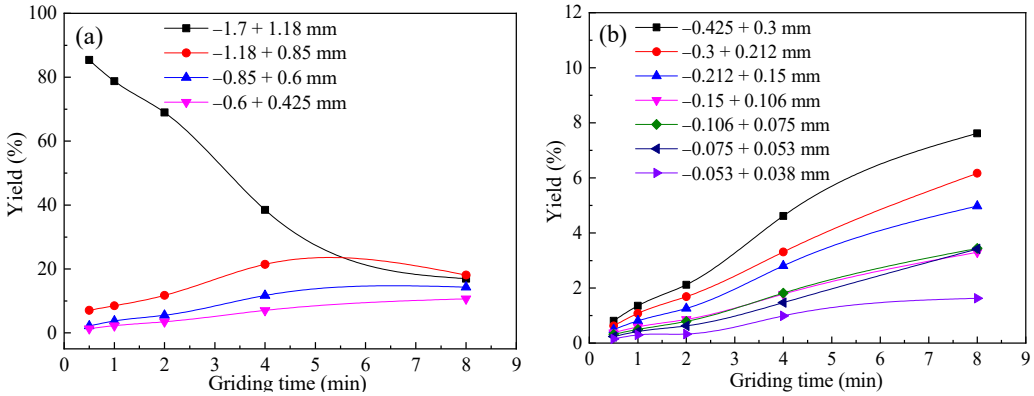

Figure 10. The variation in product yield with time for pyrrhotite with the feed particle size of −1.7 + 1.18 mm: (**a**) +0.425 mm particle size, (**b**) −0.425 mm particle size.

From Figure 8, it can be seen that pyrrhotite with the feed particle size of −3.35 + 2.36 mm is crushed to products of various particle sizes after impact grinding. Among them, the yield of the −2.36 + 1.7 mm, −1.7 + 1.18 mm, and −1.18 + 0.85 mm particle sizes is higher, with the highest yield being 19.80%, 18.27%, and 9.13%, respectively. The highest yield of the other particle sizes is 5.54%. As evident in Figure 8, with an extensive range for the ordinate, the yield curve of the −0.85 + 0.6 mm particle size is very smooth. With the expansion of the ordinate scale, as depicted in Figure 8b, the yield for each particle size at the 8 min mark does not rise above 3.72%, and the yield curve is smoother. This indicates that the generation rate of these particle sizes of pyrrhotite under impact grinding is slower, but faster than that of quartz with the same particle size.

From Figure 9, it can be seen that the pyrrhotite with the feed particle size of −2.36 + 1.7 mm is broken into particles with a more uniform distribution than that with the feed particle size of −3.35 + 2.36 mm. For the same product particle size, the yield of the −2.36 + 1.7 mm feed is higher than that of the −3.35 + 2.36 mm feed, and the generation rate is also faster. Compared with the quartz, the generation rate curve of the pyrrhotite with particle sizes of −0.425 mm generated by crushing has a more obvious change in its trend, and its generation rate is faster. This is because pyrrhotite has a lower hardness than quartz, so it is easier to break it under impact to produce products of various particle sizes.

From Figure 10, it can be seen that the pyrrhotite with the feed particle size of −1.7 + 1.18 mm is broken into more uniform products of each particle size. For each product particle size of −0.425 mm, the pyrrhotite has a higher yield than the quartz, and the variation trend of the formation rate curve is more significant. Among the three feed particle sizes, the E_{cs} of the −1.7 + 1.18 mm feed is 6.31 kWh/t, and the E_{cs} values of the −3.35 + 2.36 mm and −2.36 + 1.7 mm feeds are 0.81 kWh/t and 2.23 kWh/t, respectively. Therefore, the fastest rate is obtained when crushing the pyrrhotite with smaller feed particle sizes into each particle size.

4. Conclusions

The following conclusions were deduced from this study:

(1) According to the JK drop weight test method, based on the impact test data, the break distribution functions of quartz and pyrrhotite were solved using Matlab programming and Origin function-fitting mathematical methods. Based on batch-grinding test data, the selection functions of quartz and pyrrhotite under different conditions were obtained using the zero-order yield method, and the relationship between the selection functions of different mineral samples and grinding time was established.

(2) Based on the population balance dynamics simulation of grinding, using the break distribution function and selection function of mineral samples, the particle size distribution results of grinding products of quartz and pyrrhotite under impact action were obtained, and the impact grinding characteristics of these two minerals were obtained.

(3) The selection function of quartz and pyrrhotite decreases with the prolongation of the grinding time, and the selection function of a coarse particle size is significantly different from that of a fine particle size. At the same time, the selection function decreases as the feed particle size decreases. The smaller the feed particle size, the lower the probability of it being broken.

(4) The E_{cs} of quartz and pyrrhotite in different feed particle sizes in the mill is different, and under the same feed particle size conditions, the E_{cs} of pyrrhotite is lower than that of quartz. This means that the degree of mineral fragmentation is closely related to the impact energy, feed particle size, and mineral properties.

Author Contributions: Conceptualization, J.Y. and S.M.; Data curation, X.Y. and H.L.; Formal analysis, Z.L. and P.Z.; Funding acquisition, S.M.; Investigation, H.L. and X.Y.; Methodology, J.Y. and S.M.; Project administration, J.Y. and X.Y.; Validation, H.L. and X.Y.; Writing—Original draft, H.L. and J.Y.; Writing—Review and editing, J.Y. and S.M. All authors have read and agreed to the published version of the manuscript.

Funding: This research was funded by the National Natural Science Foundation of China (No. 52274258, No. 51874105).

Institutional Review Board Statement: Not applicable.

Informed Consent Statement: Not applicable.

Data Availability Statement: The data presented in this study are available on request from the corresponding author. The data are not publicly available due to the privacy of the experimental data.

Conflicts of Interest: The authors declare no conflicts of interest.

References

1. Hashim, S.F.S.; Hussin, H. Effect of grinding aids in cement grinding. *J. Phys. Conf. Ser.* **2018**, *1082*, 012091. [CrossRef]
2. Wang, Z.W.; Liu, Q.S. Failure criterion for soft rocks considering intermediate principal stress. *Int. J. Min. Sci. Technol.* **2021**, *31*, 565–575. [CrossRef]
3. Camalan, M. Correlating common breakage modes with impact breakage and ball milling of cement clinker and chromite. *Int. J. Min. Sci. Technol.* **2020**, *30*, 901–908. [CrossRef]
4. Musa, F.; Morrison, R. A more sustainable approach to assessing comminution efficiency. *Miner. Eng.* **2009**, *22*, 593–601. [CrossRef]
5. Napier-Munn, T. Is progress in energy-efficient comminution doomed. *Miner. Eng.* **2015**, *73*, 1–6. [CrossRef]
6. Norgate, T.; Haque, N. Energy and greenhouse gas impacts of mining and mineral processing operations. *J. Clean. Prod.* **2010**, *18*, 266–274. [CrossRef]
7. Michaux, S.; Djordjevic, N. Influence of explosive energy on the strength of the rock fragments and SAG mill throughput. *Miner. Eng.* **2005**, *18*, 439–448. [CrossRef]
8. Nagaraj, D.R. Reagent selection and optimization the case for a holistic approach. *Miner. Eng.* **2005**, *18*, 151–158. [CrossRef]
9. Xiao, X.; Zhang, G.; Feng, Q.; Xiao, S.; Huang, L.; Zhao, X.; Li, Z. The liberation effect of magnetite fine ground by vertical stirred mill and ball mill. *Miner. Eng.* **2012**, *34*, 63–69. [CrossRef]
10. Rabieh, A.; Eksteen, J.; Albijanic, B. Galvanic interaction of grinding media with arsenopyrite and pyrite and its effect on gold cyanide leaching. *Miner. Eng.* **2018**, *116*, 46–55. [CrossRef]
11. Chai, T.Y.; Qin, S.J.; Wang, H. Optimal operational control for complex industrial processes. *Annu. Rev. Control* **2014**, *38*, 81–92. [CrossRef]
12. Gorman, M.R.; Dzombak, D.A. A review of Sustainable mining and resource management: Transitioning from the life cycle of the mine to the life cycle of the mineral. *Resour. Conserv. Recycl.* **2018**, *137*, 281–291. [CrossRef]
13. Leistner, T.; Embrechts, M.; Leißner, T.; Chelgani, S.C.; Osbahr, I.; Mockel, R.; Peuker, U.A.; Rudolph, M. A study of the reprocessing of fine and ultrafine cassiterite from gravity tailing residues by using various flotation techniques. *Miner. Eng.* **2016**, *96*, 94–98. [CrossRef]
14. Huang, K.Q.; Xiao, C.H.; Wu, Q.M. Application of accurate ball-load-addition method in grinding production of some tailings. *Adv. Mat. Res.* **2014**, *962*, 771–774. [CrossRef]
15. Kotake, N.; Kuboki, M.; Kiya, S.; Kanda, Y. Influence of dry and wet grinding conditions on fineness and shape of particle size distribution of product in a ball mill. *Adv. Powder Technol.* **2011**, *22*, 86–92. [CrossRef]
16. Peng, Y.; Grano, S. Effect of Iron Contamination from Grinding Media on the Flotation of Sulphide Minerals of Different Particle Size. *Int. J. Miner. Process.* **2010**, *97*, 1–6. [CrossRef]

17. Ma, S.J.; Li, H.J.; Shuai, Z.C.; Yang, J.L.; Deng, X.J.; Xu, W.Z. Research on grinding law and grinding parameters optimization of polymetallic complex ores. *Minerals* **2022**, *12*, 1283. [CrossRef]
18. Altintas, Y.; Weck, M. Chatter stability of metal cutting and grinding. *Ann. CIRP* **2004**, *53*, 619–642. [CrossRef]
19. Daito, M. Throughfeed centerless grinding—Issues on size control and its improvement. *Tool Eng.* **2004**, *1*, 85–91.
20. Santosh, T.; Soni, R.K.; Eswaraiah, C.; Rao, D.S.; Venugopal, R. Optimization of Stirred Mill Parameters for Fine Grinding of PGE Bearing Chromite Ore. *Part. Sci. Technol.* **2020**, *39*, 663–675.
21. Yang, J.L.; Shuai, Z.C.; Zhou, W.T.; Ma, S.J. Grinding optimization of cassiterite-polymetallic sulfide ore. *Minerals* **2019**, *9*, 134. [CrossRef]
22. Epstein, B. Logarithmico-Normal distribution in breakage of solid. *Ind. Eng. Chem.* **1948**, *40*, 2289–2291. [CrossRef]
23. Sedlatschek, K.; Bass, L. Contribution to the theory of milling processes. *Powder Metal. Bull.* **1953**, *6*, 148–153.
24. Broadbent, S.R.; Callcott, T.G. Coal breakage processes: I. A new analysis of coal breakage processes. *J. Inst. Fuel* **1956**, *29*, 524–528.
25. Gaudin, A.M.; Meloy, T.P. Minerals beneficiation-model and a comminution distribution equation for repeated fracture. *Trans. AIME* **1962**, *223*, 43–56.
26. Reid, K.J. A solution to the batch grinding equation. *Chem. Eng. Sci.* **1965**, *20*, 953–963. [CrossRef]
27. Kelsall, D.F.; Reid, K.J.; Restarick, C.J. Continuous grinding in a small wet ball mill Part I. A study of the influence of ball diameter. *Powder Technol.* **1968**, *1*, 291–300. [CrossRef]
28. Meloy, T.P.; Gumtz, G.D. The fracture of single, brittle, heterogeneous particle-statistical derivation of the mass distribution equation. *Powder Technol.* **1969**, *2*, 207–214. [CrossRef]
29. Austin, L.G. Introduction to the mathematical description of grinding as a rate process. *Powder Technol.* **1971**, *5*, 1–17. [CrossRef]
30. Morozov, E.F.; Shumailov, V.K. Mathematical modeling of closed cycles of ball grinding. *Sov. Min. Sci.* **1986**, *22*, 56–65. [CrossRef]
31. Nikolov, S. A performance model for impact crushers. *Miner. Eng.* **2002**, *15*, 715–721. [CrossRef]
32. Shi, F. A review of the applications of the JK size-dependent breakage model part 3: Comminution equipment modelling. *Int. J. Miner. Process.* **2016**, *157*, 60–72. [CrossRef]
33. Deniz, V. Effects of mill speed on kinetic breakage parameters of four different particulate pumices. *Part. Sci. Technol.* **2013**, *31*, 101–108. [CrossRef]
34. Umucu, Y.; Deniz, V.; Cavirli, S. A new model for comminution behavior of different coals in an impact brusher. *Energy Sources* **2014**, *36*, 13–16.
35. JK Tech. *JkSimMet User Manual—Steady State Mineral Processing Simulator*; JK Tech Pty Ltd.: Brisbane, Australia, 2003.
36. Sun, R.G.; Gao, Y.; Yang, Y. Leaching of heavy metals from lead-zinc mine tailings and the subsequent migration and transformation characteristics in paddy soil. *Chemosphere* **2021**, *291*, 132792. [CrossRef] [PubMed]
37. Leung, K. An Energy Based Ore Specific Model for Autogenous and Semi-Autogenous Grinding. Ph.D. Thesis, School of Engineering, The University of Queensland, Brisbane, Australia, 1987.
38. Napier-Munn, T.J.; Morrell, S.; Morrison, R.D.; Kojovic, T. *Mineral Comminution Circuits: Their Operation and Optimization*; JKMRC and the University of Queensland Publishing: Indooroopilly, Australia, 2005.
39. Zou, Y.R.; Luo, L.F. Application of JKSimMet software in selection of semi-autogenous grinding mill. *Nonferrous Metall. Equip.* **2015**, *1*, 20–25.
40. Cuhadaroglu, D.; Samanli, S.; Kizgut, S. The effect of grinding media shape on the specific rate of breakage. *Part. Part. Syst. Charact.* **2008**, *25*, 465–473. [CrossRef]
41. Simba, K.P.; Moys, M.H. Effects of mixtures of grinding media of different shapes on milling kinetics. *Miner. Eng.* **2014**, *61*, 40–46. [CrossRef]
42. Narayanan, S.S.; Whiten, W.J. Breakage characteristics for ores for ball mill modeling. *Proc. Aust. Inst. Min. Metallurgy* **1983**, *286*, 31–39.
43. Pauw, O.C.; Mare, M.S. The determination of optimum imact breakage routes for an ore. *Powder Technol.* **1988**, *54*, 3–13. [CrossRef]
44. Bourgeois, F. Micro-Scale Modelling of Comminution Processes. Ph.D. Thesis, University of Utah, Salt Lake City, UT, USA, 1993.
45. Austin, L.G.; Shoji, K.; Bell, D. Rate equations for non-linear breakage in mills due to material effects. *Powder Technol.* **1982**, *31*, 127–133. [CrossRef]
46. Herbst, J.A.; Fuerstenau, D.W. Mathematical simulation of dry ball milling using specific power information. *Trans. AIME* **1973**, *254*, 343–348.
47. Deniz, V. A new size distribution model by t-family curves for comminution of limestones in an impact crusher. *Adv. Powder Technol.* **2011**, *22*, 761–765. [CrossRef]
48. Genç, Ö.; Benzer, A.H. Single particle impact breakage characteristics of clinkers related to mineral composition and grindability. *Miner. Eng.* **2009**, *22*, 1160–1165. [CrossRef]
49. Genç, Ö. Analysis of grinding media effect on specific breakage rate function of particles in a full-scale open circuit three-compartment cement ball mill. *Miner. Eng.* **2015**, *81*, 10–17. [CrossRef]

50. Deniz, V. The effect of mill speed on kinetic breakage parameters of clinker and limestone. *Cem. Concr. Res.* **2004**, *34*, 365–1371. [CrossRef]
51. Mulenga, F.K.; Moys, M.H. Effects of slurry filling and mill speed on the net power draw of a tumbling ball mill. *Miner. Eng.* **2014**, *56*, 45–56. [CrossRef]